Int J Earth Sci (Geol Rundsch) (2016) 105:2097–2110
DOI 10.1007/s00531-015-1259-y

ORIGINAL PAPER

Strain and flow in the metamorphic core complex of Ios Island (Cyclades, Greece)

Marcel Mizera[1,3] · **Jan H. Behrmann**[2]

Received: 12 May 2015 / Accepted: 5 October 2015 / Published online: 27 October 2015

Abstract We have analysed strain and flow kinematics in the footwall of the South Cyclades Shear Zone (SCSZ), an important tectonic boundary within the Attic-Cycladic Crystalline Complex exposed on Ios Island, Cyclades, Aegean Sea. Coarse-grained augen gneisses in the basement unit flooring the SCSZ and forming a metamorphic core complex are excellently suited to measure finite strain using the Fry method and estimate the vorticity number (W_k) of flow with the "blocked-object" method. The results show that Oligo-Miocene exhumation of the basement unit during extension brought approximately 70 % N–S crustal stretching and up to 40 % subvertical shortening in a plane strain environment ($k = 0.99$). Linear down-section strain decrease constrains a zone of contact deformation of the SCSZ of about 1.5 km thick. Kinematic vorticity number estimates suggest little deviation from pure shear ($W_k = 0.26$). Finite strain and W_k are not correlated, indicating that the Ios basement and the overlying cover units were stretched compatibly. While the SCSZ is a localized zone of high strain, net displacement, however, may be restricted to about ten kilometres. This has important repercussions on large-scale tectonic models for extension in the Aegean.

Keywords South Cyclades Shear Zone · Thrust · Detachment · Aegean Sea · Metamorphic core complex · Ios

Introduction

Metamorphic core complexes (MCCs), first identified in the Tertiary Basin and Range Province in the western USA (Coney 1980), are characteristic features of extensional deformation in initially thickened crust (e.g. Huet et al. 2010). The detachment—a low-dipping gliding plane between a brittlely deforming low-grade metamorphic or unmetamorphic upper and a ductilely deforming metamorphic lower crust—is the most spectacular and controversial feature of a MCC (e.g. Lister and Davis 1989). Since the first interpretation of the Cycladic islands Ios and Naxos, Greece, as MCC (Lister et al. 1984), views on the dynamics and evolution of the overriding plate in the Hellenic subduction system have changed considerably. Because the subduction zone is retreating southward, upper plate extension is moving with time, as is arc magmatism. One result is a complex system of detachments (Fig. 1) with variable kinematics in space and time (see, e.g., Huet et al. 2010; Kumerics et al. 2005; Ring et al. 2010; Grasemann et al. 2012 for recent discussions of the topic). Today, the Cyclades islands mainly expose the footwall parts of MCC. The upper units are mostly missing on-land in the Aegean region and especially on Ios, making the overall geological structure and distribution of tectonic units hard to reconstruct. Therefore, significant information about the strain and the kinematics associated with detachment

This is a contribution to Eastern Med. Tectnonics edited by Xypolias et al.

✉ Marcel Mizera
marcel.mizera@vuw.ac.nz

[1] Institut für Geowissenschaften, Christian-Albrechts-Universität, Ludewig-Meyn-Str. 10, 24118 Kiel, Germany

[2] GEOMAR Helmholtz-Zentrum für Ozeanforschung, Wischhofstr. 1-3, 24148 Kiel, Germany

[3] School of Geography, Environment, and Earth Sciences, Victoria University of Wellington, Cotton Building, CO418, Kelburn Campus, Wellington 6012, New Zealand

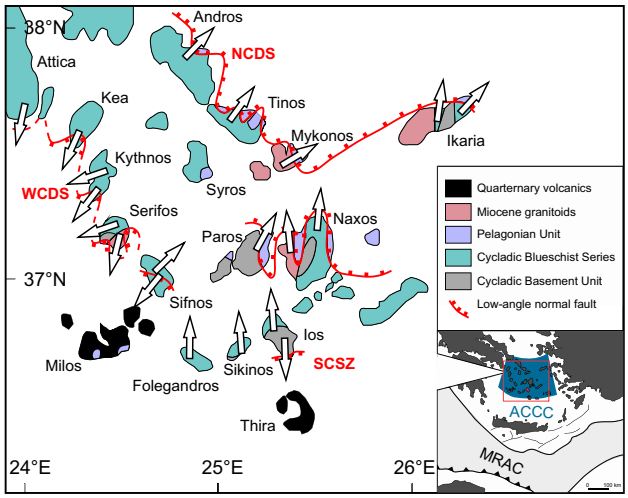

Fig. 1 Structural map of the Cyclades showing the main detachment systems and associated kinematic directions (modified after Huet et al. 2010; Grasemann et al. 2012). *WCDS* West Cycladic Detachment System; *NCDS* North Cycladic Detachment System; *SCSZ* South Cyclades Shear Zone. Overview map of the Eastern Mediterranean indicates the Attic-Cycladic Crystalline Complex (ACCC; *blue shaded area*) and the Mediterranean Ridge Accretionary Complex (MRAC; *grey shaded area*)

operation needs to come from the footwall units. These are well exposed in the Cyclades and offer important insights into the ductile flow kinematics of the MCC. The South Cyclades Shear Zone (SCSZ) on Ios Island separates the Cycladic Basement Unit (BU in the following) and the Cycladic Blueschist Series (CBS in the following). It has been interpreted as a major extensional detachment (e.g. Vandenberg and Lister 1996). However, Huet et al. (2009) point out that the presence of high-pressure rocks in the CBS speaks in favour of an origin of the SCSZ as an overthrust.

At this point, the question arises which of the two interpretations are correct and can fully account for the deformational and metamorphic histories of the rocks involved in the tectonic processes of either overthrusting or subhorizontal extension. Extensional detachments leave distinctive strain patterns mainly in the hangingwall units, like listric normal fault systems and tilted blocks. In the footwall, there is the potential for coaxial subhorizontal stretching (e.g. Kilias et al. 1999). Tectonostratigraphic duplication, imbricate thrusting, and lateral ductile shortening, on the other hand, are diagnostic of overthrusting (e.g. Boyer and Elliott 1982).

Here, we present an analysis of strain and flow kinematics in the lower-plate basement (BU) of Ios, Cyclades, Greece. The aim is to contribute new evidence regarding the origin and nature of the contact between the BU and the CBS. We constrain a tectonic model for strain localization and shear zone operation on Ios and discuss implications for Neogene extensional kinematics in the hangingwall of the Hellenic subduction zone.

Geological setting

The Cycladic archipelago

Ios Island forms part of the Attic-Cycladic Crystalline Complex (ACCC; Fig. 1), one of the key structural features of the Aegean back-arc. Exhumation was triggered by the southward retreat of the subducting African slab (Le Pichon and Angelier 1979). The ACCC can be traced from south-east Euboea eastwards over the Cycladic islands to Ikaria and Samos. The mainly Mesozoic tectonic-metamorphic units of the ACCC belong to the Hellenide nappe stack, which was formed during convergent tectonics in the Eocene (e.g. Jacobshagen 1986). From bottom to top, the tectonic units of the Cycladic Archipelago are as follows (Fig. 1): (1) the BU, a pre-Alpine basement comprising granites, paragneisses, and orthogneisses found on the southern Cyclades (Ios, Sikinos; van der Maar 1980) and Samos (Ring et al. 1999) and metamorphosed to migmatites on the central Cyclades (Naxos and possibly Paros; Andriessen et al. 1987; Jacobshagen 1986 and references therein); (2) the intermediate CBS made up of metapelites, marbles, and metabasites and present on most of the Cycladic islands (Jansen and Schuiling 1976; Dürr et al. 1978; Schliestedt et al. 1987); (3) the uppermost allochthonous Pelagonian Unit (PU) with ophiolitic remnants of the Vardar Ocean and non-metamorphosed Miocene sediments located in the hangingwall of the MCCs of the northern (Andros, Tinos, Mykonos) and central Cyclades (Naxos and Paros; Jolivet et al. 2012; Huet et al. 2009 and reference therein).

Isotopic dating in the BU suggests a complex pre-Alpine origin with Variscan (305–295 Ma) and possible pre-Variscan (~500 Ma) ages (e.g. Henjes-Kunst and Kreuzer 1982; Seidel et al. 2006). The Alpine history of the Cyclades is described by two major tectonometamorphic events which have affected the BU and the overlying CBS: (M_1) a subduction-related Eocene high-pressure–low-temperature (HP–LT) eclogite/blueschist facies metamorphism, well documented in the marbles and schists of the CBS but poorly recorded in the BU; (M_2) an Oligo-Miocene (25–16 Ma) Barrovian-type greenschist facies metamorphism, which affected the BU and the overlying CBS (e.g. Jansen and Schuiling 1976; Altherr et al. 1982; Henjes-Kunst and Kreuzer 1982; Andriessen et al. 1987; Vandenberg and Lister 1996; Huet et al. 2009). Low-pressure–high-temperature contact metamorphism occurs locally, related to late Miocene granitoids (M_3; 22–10 Ma, Altherr et al. 1982). The succession of the metamorphic events tracks the burial and exhumation of the BU and the CBS (Huet et al. 2009).

The upper Cycladic nappe (PU) lacks high-pressure metamorphism and is separated from the BU and CBS by detachment fault zones (e.g. Lister et al. 1984; Huet et al. 2009). Shearing is top-to-northeast on the northern (Andros, Mykonos, Tinos, Ikaria) and top-to-north on the central Cyclades (Naxos, Paros; Huet et al. 2010). Only remnants of the PU are preserved on the western (Kea, Kithnos, Serifos; Grasemann et al. 2012) and completely missing on the southern Cyclades (Sikinos, Ios; Vandenberg and Lister 1996; Huet et al. 2009). Sense of shear on brittle–ductile extensional faults in the western Cyclades is top-to-southwest (Grasemann et al. 2012; Huet et al. 2009). The most complex kinematic pattern is found on Ios Island with both top-to-north and top-to-south senses of shear (Lister et al. 1984; Vandenberg and Lister 1996; Forster and Lister 1996; Huet et al. 2009).

Geology and deformation history of Ios Island

Descriptively, Ios Island is a mantled gneiss dome (Fig. 2; van der Maar 1980) forming the basement (the BU), covered by a marble–schist series (the CBS).

The BU is made up of a variably deformed metagranite augen gneiss core, interleaved with and covered by metasedimentary garnet–mica schists (van der Maar 1980; see also Fig. 2). Schist–gneiss contacts are distinct without any transition zone. Pre-Variscan radiometric ages (~500 Ma) of the metagranitic bodies are interpreted as intrusion ages (Henjes-Kunst and Kreuzer 1982; Andriessen et al. 1987). Radiometric cooling ages determined from the garnet–mica schists are thought to date a Variscan (M_0) metamorphic event (~300 Ma, Henjes-Kunst and Kreuzer 1982). Alpine orogeny has erased all other evidence for this event (Vandenberg and Lister 1996).

The BU–CBS contact is sharp. At an early stage, the contact between the two units was interpreted to represent a stratigraphic time gap (van der Maar 1980), but was later recognized to host a major shear zone (see, e.g., Vandenberg and Lister 1996). The overlying CBS comprises calcite and dolomite marbles, metapelites, and metabasalts (now blueschists and greenschists, but locally also preserved as eclogites) with scattered inclusions of ultramafic rocks (van der Maar 1980). The close association of high-pressure rocks resembling an ophiolitic melange and those resembling a carbonate platform indicates that the CBS formed part of a subduction complex in the Eocene, but maybe as young as 30 Ma (i.e. earliest Oligocene; see, e.g., Ring et al. 2010), with pressure estimates in the range of 9–15 kbar during high-pressure metamorphism (M_1; see Henjes-Kunst 1980; van der Maar 1980; van der Maar and Jansen 1983). The overprinting Miocene greenschist facies metamorphism (M_2) is characterized by the growth of chlorite, albite, biotite, and garnet, (380–420 °C; 5–7 kbar; Henjes-Kunst 1980; van der Maar 1980).

Three main phases of fabric generation subdivided into five ductile deformation events (D_1–D_5 from old to young) were identified by previous workers (Vandenberg and Lister 1996; Forster and Lister 1996; Lister and Keay 1996; Baldwin and Lister 1998; Forster and Lister 1999a, b). We concur with this scheme and refer to it in the following description. D_1 microfabrics are locally preserved in garnet–mica schists of the BU and are overprinted by a ubiquitous and penetrative D_2 foliation, which also is the main fabric element in the augen gneisses of the BU (Figs. 2, 3). This deformation produced a strong N–S trending stretching lineation (Fig. 2) and probably accommodated most of the bulk ductile strain in the rocks exposed on Ios. D_2 foliations are also present in the CBS unit and are therefore interpreted to be of Alpine age. Because of the lack of D_2 kinematic indicators there, Vandenberg and Lister (1996) inferred that ductile flow during D_2 was largely coaxial in the CBS.

The D_3–D_5 sequence of deformation events started during retrograde greenschist facies metamorphism and is associated with subhorizontal extension. D_3 is marked by tight to isoclinal folds with non-penetrative axial planar differentiated crenulation cleavage. D_4 is post-greenschist grade and is localized in 10- to 500-m-scale shear zones associated with the younger part of N–S extension and the development of the SCSZ (Fig. 2). Within the SCSZ proper, D_4 kinematic indicators show dominant top-to-south shearing. Several discrete low-angle extensional shear zones of late-stage D_4 age have been identified: the Ios Detachment Fault (IDF; Fig. 2) truncating SCSZ fabrics, the André Fault (AF; Fig. 2) crosscutting the IDF, and the Coastal Fault System (CFS; Fig. 2) on the NW coast of Ios island (Forster and Lister 1999a). Additionally, Forster and Lister (1999a) describe a top-to-north shear zone within the BU overprinting D_2 fabrics (see analysis of Vandenberg and Lister, 1996) in the northern part of the island (Headland Shear Zone, HSZ; see Fig. 2), which was active at about 19–18 Ma (Thomson et al. 2009). This age puts it into direct temporal context with D_2 shearing. The youngest (D_5) ductile deformation relates to the structural doming of the island and is expressed by local N–S trending upright folds at outcrop scale (see also Thomson et al. 2009).

Methods

For the application of the Fry method (Fry 1979a, b), images of suitably oriented outcrop faces (parallel to principal planes of the strain ellipsoid) in the basement augen gneisses of Ios Island were used (see examples in Fig. 3). In most cases, two sections were analysed (usually the XZ and YZ ones), and axial ratios of the third principal section were calculated from these. The Fry plots (insets in Fig. 3)

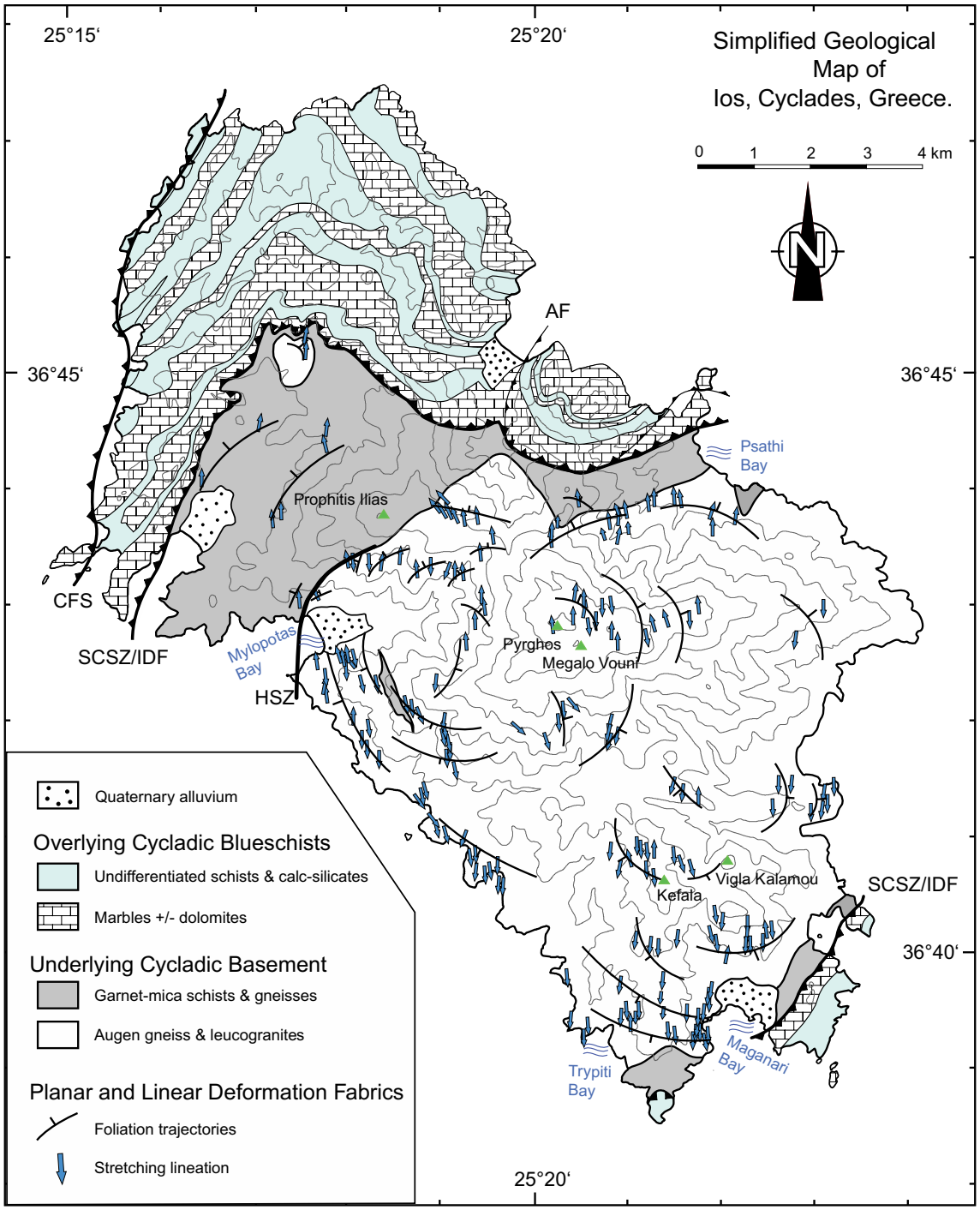

Fig. 2 Simplified geological map of Ios (modified after van der Maar et al. 1981; Thomson et al. 2009; Huet et al. 2009, and also based on own observations). Shown are major rock types, D_2 foliation trajectories, stretching lineations, and major extensional shear zones (*AF* André Fault; *CFS* Coastal Fault System; *HSZ* Headland Shear Zone; *SCSZ/IDF* South Cyclades Shear Zone/Ios Detachment Fault). See text

provide graphical solutions to the centre-to-centre method. The bulk rock strain is determined by using the redistribution of object centres (i.e. ooid centres, pebble centres, sand grain centres, porphyroblasts, porphyroclasts) in the deformed rock and the distances between these points as extended line elements (e.g. Ramsay and Huber 1983). We found that the spatial distributions of augen fabrics in the gneisses were excellently suited to calculate the finite

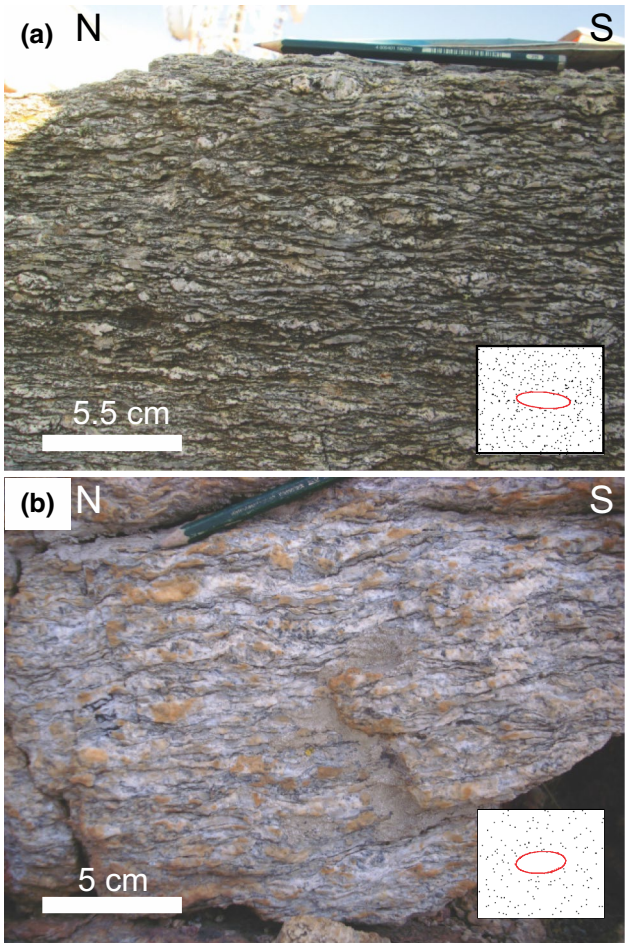

Fig. 3 Two examples of deformed granite gneisses from the BU, the rock type on which this study is based on. Exposed faces of the outcrops show XZ principal sections of finite strain. *Insets* show the strain *ellipses* determined by using the Fry method. **a**: Augen gneiss (Loc. X10_17) located at Pyrghos, the highest point of the dome ($N = 64$; $R_{XZ} = 3.44$). **b** Coarse-grained feldspathic gneiss (Loc. X20_03) located near Trypiti Bay ($N = 37$; $R_{XZ} = 2.31$)

strains. To construct the Fry plots, we used the computer program GeoFryPlot 3.1 by Holcombe (2004).

Application of the Fry method as a tool to measure strain is restricted to initial spatial distributions of porphyroclasts that do not have a Poisson random distribution. A homogeneous distribution of K-feldspars initially crystallized from a melt, and now present as porphyroclasts, is probably a reasonable assumption, as well as approximately homogeneous plastic deformation at outcrop scale. If initial distribution was not homogeneous, the result of the Fry analysis would not show as in Fig. 3. Inhomogeneous deformation at outcrop scale, on the other hand, would be readily visible as shear zones. Errors, of course, may result from inaccurate determination of the object's centres. The geometric centres of porphyroclasts were defined by the intersection points of the longest and shortest axis. This can be challenging especially when the objects are not perfectly elliptical. Further errors occur when fitting the strain ellipse to the area of point vacancy in the centres of the Fry plots, which is necessarily a visual and subjective procedure. To avoid errors caused by mismatches between viewing direction of the camera and the principal plane of the strain ellipsoid used for analysis, care was taken to keep this angle of mismatch at less than 20°. This restricts errors to less than a few per cent. Thus, the Fry method offers a quick and fairly reliable estimate of the finite strain, keeping in mind that the strains are matrix strains at outcrop scale, which need not be reflected by the shapes of the K-feldspar porphyroclasts.

Porphyroclasts embedded in rocks with a ductilely deforming matrix can provide important information regarding the vortical component of flow. The topic was pioneered by Ghosh and Ramberg (1976) and has later been applied in a multitude of studies (for a review, see, e.g., Xypolias 2010). The Jeffery model (Jeffery 1922) provides the theoretical foundation. Two of the important underlying assumptions are that porphyroclasts should behave as isolated rigid inclusions and that deformation should not localize either through slipping or through a fluid film around the porphyroclast/matrix interface (e.g. Johnson et al. 2009). Isolation (see, e.g., Piazolo et al. 2002) may be an issue in the rocks studied, with K-feldspar porphyroclast contents up to about 30 % (see Fig. 3), and result in slight underestimates of the kinematic vorticity number W_k for objects with aspect ratios of about 2–3 (Fig. 3). Slipping would be the case when much of the matrix deformation is located in shear bands. Therefore, we have excluded outcrops with strong shear band fabrics from our analysis. Figure 3 shows examples of porphyroclast-bearing outcrops with weak shear band fabrics that, while not being ideal, we would still consider as being suitable.

The "blocked-object" method proposed by Passchier (1987) can be applied when rigid objects in a ductilely deforming matrix attain stable positions in the flow field. The long axis of the "blocked" porphyroclast defines an instantaneous stretching axis (ISA), whereby the finite stretching axis (FSA) or extensional flow apophysis (Passchier 1987) is taken to be parallel to the foliation, or the straight, distant part of the recrystallized tail. The angle η between ISA and FSA is a function of the axial ratio of the porphyroclast (B^*) and the kinematic vorticity number W_k. This relation can be expressed as follows (Passchier 1987):

$$\eta = \frac{1}{2}\arcsin\left(\frac{W_k}{B^*} * \left(\sqrt{1 - W_k^2} - \sqrt{B^{*2} - W_k^2}\right)\right) \quad (1)$$

where B^* is defined as

$$B^* = \frac{Mx^2 - Mn^2}{Mx^2 + Mn^2} \quad (2)$$

with Mx and Mn being the lengths of the object's long and short symmetry axes.

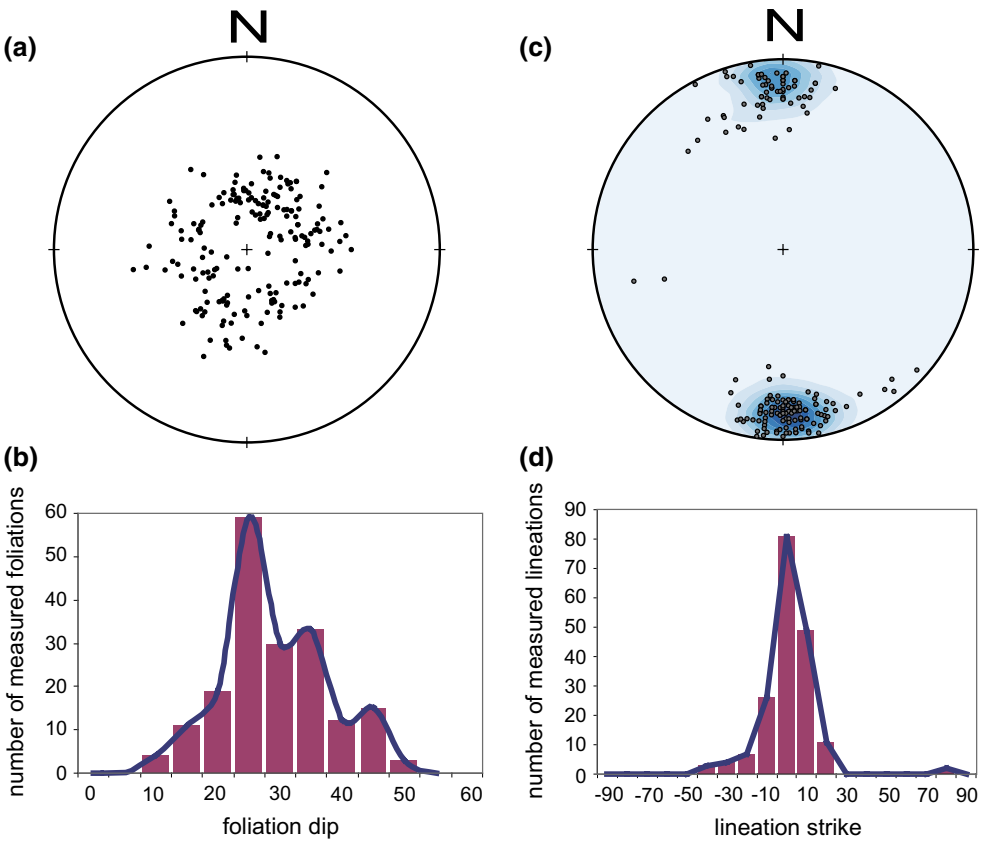

Fig. 4 Orientation distributions of planar and linear deformation fabrics attributed to D_2 in the BU. **a** Equal-area, lower hemisphere projections of poles to foliation planes; **b** *histogram* showing distribution of foliation dip angles; **c** equal-area, lower hemisphere projections of stretching lineations; **d** *histogram* showing orientation distribution of stretching lineation azimuths

Obviously, B^* is zero for spherical objects (see Eq. 2) and becomes larger with increasing aspect ratio of the blocked object. Equation 1 is only defined for nonzero values of B^*, a condition that can be checked to be applicable when examining the aspect ratios of the large feldspar clasts in Fig. 3. When $B^* < W_k$, the object will end up in permanent rotation and form a δ-clast (Passchier 1987; Behrmann 1990). The angle η and B^* can be directly read from the fabrics in the deformed rock. Equation 1 can then be solved for W_k, giving the estimates of the kinematic vorticity number for ductile flow.

The most common source of error when using the "blocked-object" method is the determination of the angle ŋ between the ISA and FSA, and the definition of the elliptical shape of the feldspar augen (B^*). Estimated vorticity numbers are systematically too low, when the viewing direction towards the porphyroclast image is not parallel to the vorticity vector (the axis around which material lines rotate; see, e.g., Iacopini et al. 2008). Behrmann (1990) showed that angular mismatches between the viewing direction and the vorticity vectors of less than 25° lead to W_k estimates up to 6 % too low. In our analysis, mismatch angles were consistently kept under 20°; i.e. the angles between viewing direction and direction of maximum finite stretching were larger than 70° in all cases. However, applying this 6 % error to our W_k data set does not substantially alter interpretations and conclusions given below.

Results

Mesoscopic planar and linear deformation fabrics

Orientations of all measured D_2 foliations in the BU unit on Ios Island are shown in the lower hemisphere, equal-area projection in Fig. 4a. Results are compatible with earlier analyses (Vandenberg and Lister 1996; Huet et al. 2009). Construction of foliation trajectories (Fig. 2) shows that the structure of Ios can be approximated as an axially symmetric dome made up of the two tectonic units BU and CBS. The flanks of the dome are dipping in all directions with moderate angles. The foliation planes commonly dip away from the centre of the island with an arithmetic mean of 27° (total range 8–50°; see Fig. 4b). Eighty-two per cent of the dip angle values are between 15° and 45°, and the standard deviation is 8.5° (Fig. 4b).

The measured D_2 stretching lineations as defined by the long axes of tailed feldspar porphyroclasts in the augen gneisses (Fig. 3) have a very distinct orientation distribution around the N–S direction (Fig. 4c, d). The values are centred around 357° azimuth with a standard deviation of

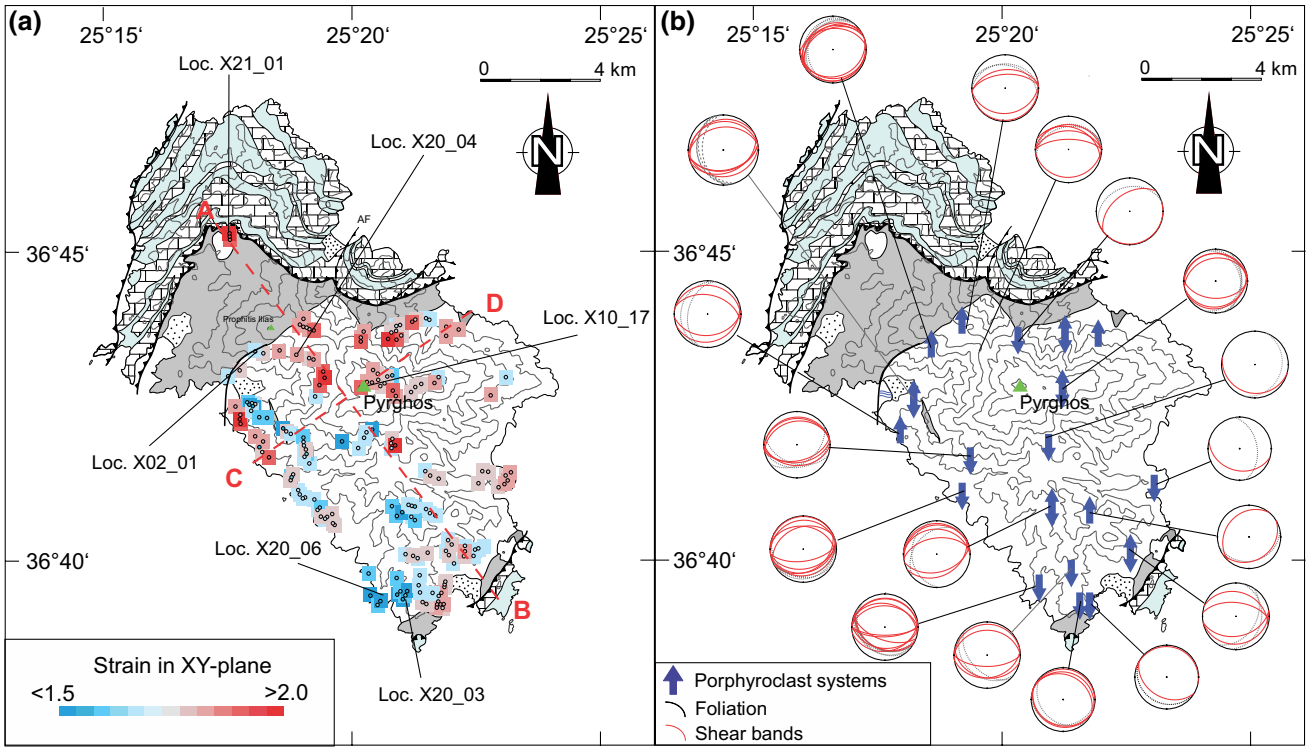

Fig. 5 Strain and flow kinematics in the BU of Ios Island. Legend for lithological units is the same as in Fig. 2. **a** Strain distribution. *Dark blue squares* low strain values; *dark red squares* high strain values. Strain is represented by values computed for the XY plane, which approximates map view. *Dots* outcrop locations; *red dashed lines* profile lines shown in Fig. 7. **b** Senses of shear from porphyroclast systems and shear bands. Conjugate and single-set shear band fabrics and associated foliations are shown as equal-area projections

14° (Fig. 4d). Nearly 85 % of the lineation trends cluster between NNW–SSE and NNE–SSW. More than 75 % of the angles of plunge are less than 30°, with an arithmetic mean of 15° and a standard deviation of 8°. In the lower hemisphere equal-area projection, the lineations are generally homogenously distributed and show low dispersion (Fig. 4c). A maximum pole density of 23.6 % is located at 180.0°/14.4°, as shown by the distribution of contours in Fig. 4c.

Strain

Strain geometry and magnitude

At map scale, strain magnitude in the BU varies from almost undeformed granitic protoliths to mylonitic augen gneisses with elongated to laminated K-feldspar augen and quartz crystal aggregates. The augen gneisses with the highest strain are located at the morphological ridges structurally beneath the garnet–mica schists (Figs. 2, 5a) and around the summit area of Ios Island (Pyrghos and Megalo Vouni, Fig. 5a; also described by Huet et al. 2009). As a data example, Fig. 3a shows a strongly deformed white–grey-coloured coarse-grained orthogneiss from locality (Loc. X10_17) near Pyrghos, with elongated centimetre-sized augen and quartz ribbons. The average strain values (arithmetic mean) around Pyrghos and Meghalo Vouni (Loc. X10_15–X10_17; Fig. 5a) are $R_{XZ} = 3.46$, $R_{YZ} = 1.87$, and $R_{XY} = 1.92$ ($k = 1.03$).

Less intensely strained rocks crop out in the core of the dome and in the southern part of the augen gneiss basement (Fig. 5a). Undeformed granites are found locally as strain enclaves, principally in the less deformed part of the dome. Figure 3b (Loc. X20_03) shows an example of moderately deformed augen gneiss. The foliation is mainly defined by K-feldspars and lenticular quartz–feldspar aggregates. Figure 3b also shows a weakly defined set of top-to-south shear bands, a feature indicative of small-scale strain partitioning frequently seen in the less strained part of the BU. The average strain values (arithmetic mean) in the moderately strained south-western part (Fig. 5a) are $R_{XZ} = 2.21$, $R_{YZ} = 1.5$, and $R_{XY} = 1.49$ ($k = 1.01$). At Loc. X20_06 (Fig. 5a), almost undeformed granite with slightly reoriented and fractured feldspar clasts occurs.

The most intensely strained rock unit in the BU is situated in the northern garnet–mica schist zone near the culmination of the north-dipping anticline of the dome

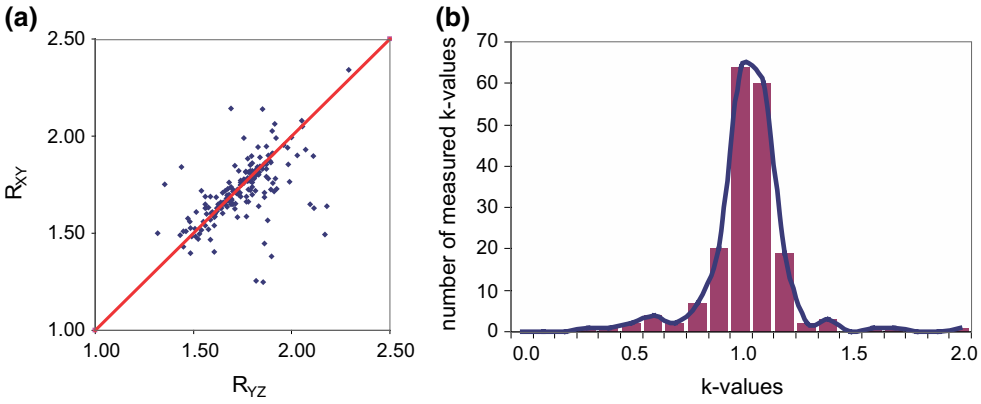

Fig. 6 Strain geometry and magnitude. **a** Flinn graph (Flinn 1962) of the data, indicating overall plane strain. **b** *Histogram* showing approximate Gaussian distribution of k values around plane strain ($k = 1$)

(Fig. 5a; Loc. X21_01). It is a dense and massive, white–grey-coloured metagranite consisting of albite, muscovite, biotite, and quartz with minor apatite and ore minerals (van der Maar 1980). This metagranite contains large microcline crystals and sometimes biotite lenses up to a few tens of centimetres. The spatial distribution of the microcline crystals was used to determine the strain with the Fry method. The average strain values (arithmetic mean) measured in this rock unit are $R_{XZ} = 4.02$, $R_{YZ} = 2.06$, and $R_{XY} = 1.97$ ($k = 0.96$).

Lenses of white fine-grained quartz–albite gneisses occur within the augen gneiss basement as small units and as a major western unit. The major western unit consists of albite, quartz, and muscovite, whereas the small units are purely made of quartz and albite. Both units are described as meta-aplites on account of mineralogical composition, the fine-grained texture, and the structural occurrence (van der Maar 1980). At Loc. X2_04 (Fig. 5a), the position fabrics of mesoscopic albite crystals were used for strain analysis. The average strain values (arithmetic mean) of this small lens are $R_{XZ} = 3.23$, $R_{YZ} = 1.78$, and $R_{XY} = 1.81$ ($k = 1.02$), which is compatible with those found in the surrounding augen gneisses.

Arithmetic means of the strains recorded were calculated for every outcrop studied. A grand total of 189 analyses were performed, and results are plotted in a Flinn graph to show the characteristics of strain geometry (Fig. 6a). Overall, deformation in the BU of Ios Island is almost perfectly plane strain, with an average k value of 0.99 (total range: 0.29–2.12) and a standard deviation of 0.2 (Fig. 6b). Almost 90 % of the data cluster in a range of k values between 0.8 and 1.2. The grand average (arithmetic mean) is $R_{XZ} = 2.98$, $R_{YZ} = 1.75$, and $R_{XY} = 1.72$. A comparison between the northern, middle, and southern parts of the island shows no significant differences. The highest strain values can be found in the central and in the northern structurally high part of the BU, whereas the lowest strain values crop out in the central-southern part (Fig. 5a).

Strain gradients

N–S and E–W profiles were constructed to calculate the depth of the studied outcrops relative to the overlying SCSZ (Fig. 7). The objective was to investigate whether there is a strain gradient away from the SCSZ into the BU. Foliation trajectories in the BU and the map attitude of the SCSZ were used for the construction. The exercise was done using our own data and all available information from the literature (van der Maar et al. 1981; Vandenberg and Lister 1996; Huet et al. 2009).

The results of the reconstructions show a gradual decrease in strain away from the SCSZ. The coefficient of correlation (R^2) of the regression line is around 0.5 for linear regression (shown in Fig. 7, bottom right) and 0.45 for exponential regression. Extrapolation of the results suggests a strain value of $R_{XZ} = 5.63$ near the contact of the SCSZ and a lower boundary of the zone of contact strain in the BU about 1500 m beneath the SCSZ. Our results also indicate that the lower boundary of the zone of contact strain is presently nowhere exposed on the surface of Ios Island, but is expected to occur around 500 m below the present outcrop of the crest of the structural dome around Pyrgos in the centre of the island (see Figs. 2, 7, 9). We interpret this downward strain gradient as reflecting the fact that deformation in the BU could indeed be related to extension and indicates the presence of a half mega-shear zone in the footwall of the SCSZ.

Flow

Kinematic indicators

Generally, three different types of shear band fabrics were observed in the BU: (1) top-to-south shear bands (weakly developed sets can be seen Fig. 3b) forming SC structures (cf. Lister and Snoke 1984), (2) conjugate sets of shear bands with E–W trending intersection lines, and (3) top-to-north shear bands, locally found to overprint the

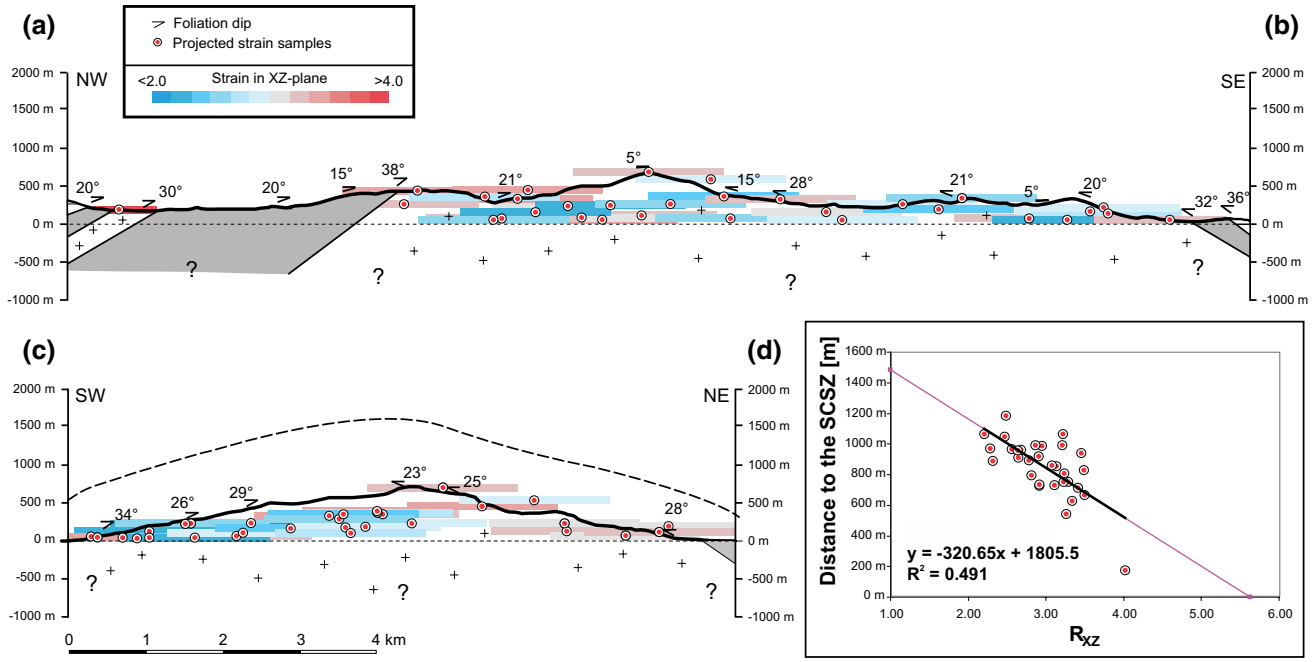

Fig. 7 SW–NE and NW–SE structural cross sections of Ios Island, based on own and literature data (van der Maar et al. 1981; Vandenberg and Lister 1996; Huet et al. 2009). Cross sections show clustered strain values (strain data in 1 km radius and <100 m height difference) from Fig. 5a and reconstruction of the SCSZ. *Dark blue squares* low strain values; *dark red squares* high strain values. *Red dots* positions of clustered outcrops used for strain analysis projected on profiles ($N = 31$). *Inset* in lower right of figure shows strain data plotted versus depth below SCSZ weighted by distance to the cross sections and results of linear regression of the data

top-to-south set. Top-to-north shear bands are mainly found in the near field of the HSZ, where top-to-north porphyroclast systems are found (see description below). Conjugate sets of shear bands, however, dominate the picture, as can be seen in Fig. 5b. Tailed sigma-type porphyroclasts of K-feldspar are ubiquitous in the augen gneisses of the BU and can contribute local sense-of-shear information. In many cases, porphyroclast fabrics are more or less symmetric, and in others they are asymmetric (Fig. 3b). Symmetric porphyroclast fabrics are abundant along the morphological N–S axis of the island around Phyrgos (Fig. 5b). Where tailed porphyroclasts are asymmetric, the sense of shear is dominantly top-to-south (see Fig. 5b). Note that arrows in Fig. 5b do not depict single observation points, but show the aggregated and averaged sense-of-shear information of all outcrops in the immediately surrounding area. The example in Fig. 3b shows asymmetrically tailed sigma porphyroclasts that indicate a top-to-north sense of shear, but was found in an area where porphyroclast fabrics predominantly indicate top-to south shearing (compare with Fig. 5b).

Whereas symmetric porphyroclasts and conjugate sets of shear bands can be taken as indicators for approximate coaxial deformation, ambiguous or conflicting cases of sense-of-shear indicators (as in Fig. 3b) obviously need explanation. The concentration of top-to-north senses of shear from porphyroclast fabrics NW of Pyrghos (Fig. 5b) can be explained by the proximity to the HSZ, which has a top-to-north normal displacement and may be associated with distributed ductile (D3) overprinting of D2 structures (see Fig. 4 in Vandenberg and Lister 1996) in the footwall.

On the other hand, the example in Fig. 3b, indicating top-to-north shearing from porphyroclasts, comes from Trypiti Bay (Fig. 2), a larger area that has otherwise a strong predominance of top-to-south indicators (Fig. 5b). Here, fabrics are tightly and recumbently refolded by D3 around NE–SW axes at outcrop scale. This can lead to a reversal of shear sense indicators that were formed pre-D3, when viewed in a N–S section (Fig. 3b). In our analysis of D2 flow vorticity, we have tried to eliminate indicators from such settings wherever we were aware of them. Figure 3b also holds important information that shear band and porphyroclast fabrics may not necessarily be syngenetic, because weakly expressed top-to-south shear bands overprint the foliation and porphyroclast fabric (near top and centre of photograph in Fig. 3b). The frequent occurrence of conjugate sets of shear bands (Fig. 5b), however, points out that shear band operation could be a reflection of near-coaxial N–S stretching (see, e.g., Platt and Vissers 1980; Behrmann 1987), which would be in line with the general geometry of the stretching fabrics in the BU (Fig. 2).

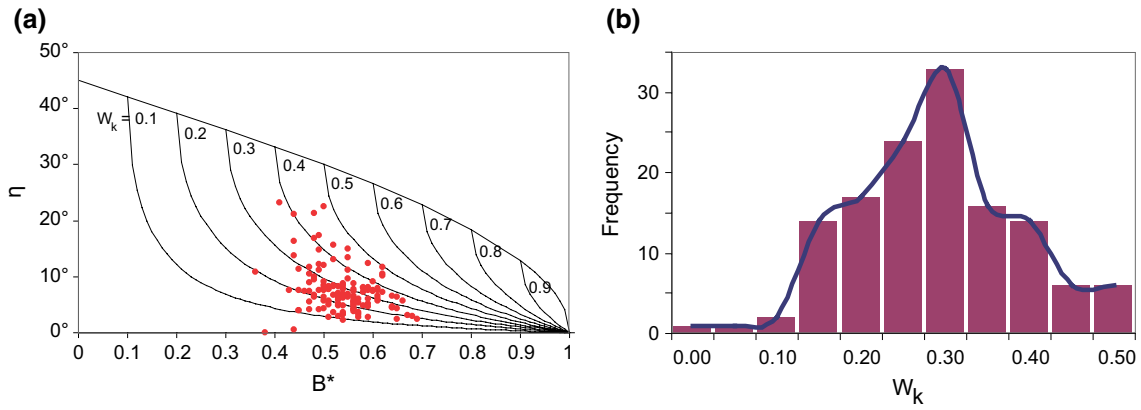

Fig. 8 Calculated kinematic vorticity numbers. **a** η-B^*—Passchier graph with the arithmetic means of W_k values from all studied outcrops. **b** Frequency distribution of W_k values

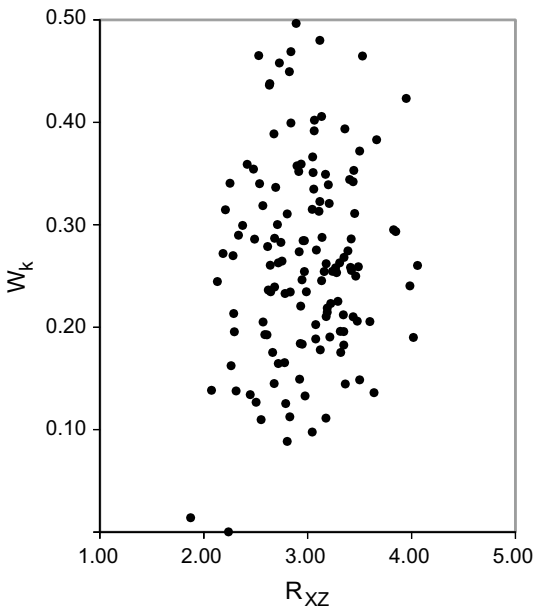

Fig. 9 Finite strain (R_{XZ}) plotted against kinematic vorticity numbers (W_k)

Kinematic vorticity number

The geometries of a total number of 1066 sigma-type porphyroclasts were analysed from all parts of the BU. Care was taken not to analyse porphyroclasts from areas showing younger fabric overprinting or from outcrops with strongly developed sets of shear bands because of the risk of geometrical modifications of the porphyroclast tails and the foliation fabric. This restriction mainly applies to the south-western part of the BU, where bulk deformation is less intense, but shear band fabrics are frequent (compare Fig. 5a, b). Values for the kinematic vorticity number W_k were found to vary between zero and 0.5. There are no examples that would suggest highly non-coaxial deformation, with values for W_k close to one. The frequency distribution of W_k shows an approximate normal distribution (Fig. 8b). The average value for W_k is 0.26, with a standard deviation of 0.09, and a potential error underestimating W_k on order of 6 % (see "Methods" section). About two-thirds of the values for W_k are in the range between 0.2 and 0.4 (Fig. 8b). Therefore, the kinematics of flow in the MCC of Ios does not deviate strongly from coaxial deformation. Plotting the finite strain against the vorticity number shows no correlation between these two values (Fig. 9).

Discussion

Large-scale strain and flow; kinematic nature of the SCSZ

The BU on Ios Island forms the core of an almost concentric dome structure (Fig. 2), which is constrained by the attitude of the second generation of foliations. As evident in Fig. 4, the dome flanks have an average dip angle of 27° (see also van der Maar 1980; van der Maar and Janssen 1983; Vandenberg and Lister 1996; Forster and Lister 1999a; Huet et al. 2009). The dome, however, does not reflect concentric stretching and vertical attenuation, as the measured stretching fabrics show a fairly constant N–S trend, indicating the direction of maximum ductile extension of the basement (see also Huet et al. 2009). Because of the plane strain nature ($k = 0.99$), the average amount of N–S stretching and subvertical attenuation of the BU can easily be calculated. Taking the arithmetic means of the principal strains X and Z, ductile deformation led to an average 72 % N–S stretching (total range 25–134 %) in the BU and reduced its tectonic thickness normal to the foliation by about 43 % (total range 24–56 %). If we assume

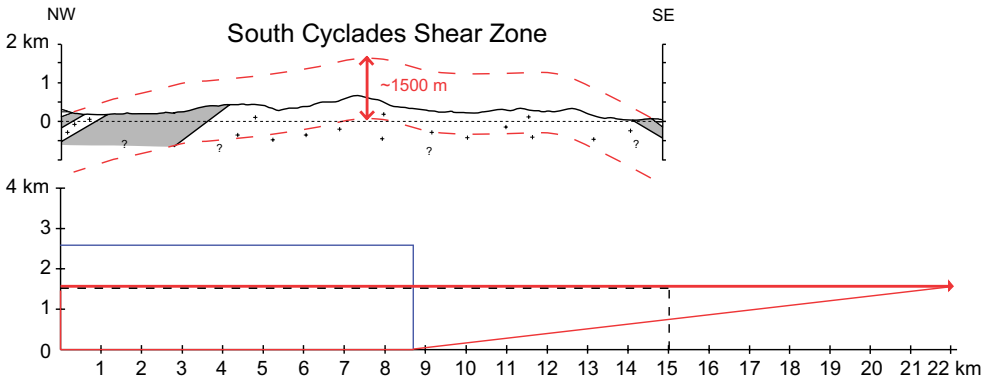

Fig. 10 Strain and kinematic model for the Ios MCC. *Top* Profile of the basement with the interpolated SCSZ (*upper dashed red line*) and the line of no-strain (*lower dashed red line*). *Bottom* Isochoric plane kinematic model for D_2 contact strain. *Black dashed box* indicates coaxially deformed reference body (15 km × 1.5 km). *Blue box* indicates reference body before deformation (8.7 km × 2.6 km). *Red box* indicates the shape of the deformed body implying upward linear strain increase to $R_{XZ} = 5.63$ at the contact of the SCSZ (*bold red line*). See text for discussion

full kinematic coupling across the SCSZ, then the overlying units must have been compatibly stretched, probably through distributed semi-ductile or (at higher crustal levels) brittle deformation. If the constraint of kinematic coupling is relaxed, the amount of vertical attenuation in the tectonic overburden may be lower and probably be closer to the values inferred from structural analysis and 1D strain modelling (Feehan and Brandon 1999) in other islands (e.g. Kumerics et al. 2005; Ring and Kumerics 2008). As the SCSZ, however, does not have the attitude of a brittle, discontinuous structure anywhere on the island (see, e.g., Vandenberg and Lister 1996), we find the assumption of kinematically coupled and compatible ductile flow a reasonable one.

The linear vertical strain gradient (Figs. 7d, 10) away from the SCSZ attests to the kinematic nature of this ductile structure (see also Huet et al. 2009) and, at the scale of the island, predicts a lower boundary of the zone of contact strain about 1500 m below the SCSZ (Fig. 10), even though there are strain enclaves and heterogeneities that perturb the picture at the 100–500 m scale (Fig. 5a; see also documentations of Vandenberg and Lister 1996; Huet et al. 2009). This heterogeneity is also characterized by the three different types of shear bands (Fig. 5b). In the case of non-coaxial deformation, top-to-south kinematic indicators are dominant in the BU (Fig. 5b), an interpretation that we share with Vandenberg and Lister (1996). However, there are extensive areas where porphyroclasts are symmetric, and two conjugate sets of shear bands are developed (Fig. 5b), an observation that is most easily interpreted as reflecting coaxial deformation. This is at variance with models for the SCSZ as a large simple shear zone that would constrain the shear zone walls to be rigid or to deform by compatible simple shear (e.g. Ramsay and Graham 1970). Coaxial stretching and/or flow with low kinematic vorticity numbers ($W_k = 0.26$ on average) structurally beneath the SCSZ means that the shear zone has changed its length compatibly with the stretching of the footwall.

Taking into account the data for strain and the kinematic vorticity number, and assuming the documented downward linear strain decrease in the BU, predictions can be made about its shape change and the length change of the SCSZ. This is done in Fig. 10, which shows that the length change of the SCSZ is 13.4 km, which adds to any displacement that may be accommodated in the shear zone itself. The distance between the no-strain-line and the SCSZ (1.5 km) and the length of the basement in the NW–SE profile (15 km) were used as a reference cross section area to describe the deformation in the principal *XZ*-plane of strain (Fig. 10, bottom). Assuming isochoric plane strain, the reference area has an unstrained size of 8.7 km by 2.6 (blue square in Fig. 10). The reference body describing the initial geometry of the area is vertically attenuated by about 1.2 km, owing to the highly coaxial nature of the deformation.

One of the important consequences of this strain and flow geometry is that the overlying CBS, containing the high-pressure metamorphic rocks, was very probably extended N–S and was vertically attenuated in a compatible fashion. This is a strain and kinematic pattern that speaks against the SCSZ and its subjacent zone of contact strain (the BU) being a thrust structure, as proposed by Huet et al. (2009). Without doubt, the CBS was tectonically emplaced on top the BU. However, the missing high-pressure assemblages in the latter indicate that this was not in a phase of compressive mountain building, and the high-pressure assemblages may have already reached mid-crustal levels by upward flow in an Eo-Hellenic subduction channel (in

the sense of Shreve and Cloos 1986; Gerya et al. 2002). Work of Behrmann and Seckel (2007) from the Small Cyclades Iraklia and Schinoussa, located to the north and structurally above Ios, shows that a high-pressure metamorphism is early in the tectonic evolution and associated with top-to-north sense of shear, probably relating to upward flow of material in a north-dipping subduction channel.

In the light of the evidence presented here, we find the interpretation of Vandenberg and Lister (1996) more likely that the SCSZ on Ios Island is a truly extensional structure that post-dated early high-pressure metamorphism in the hangingwall. In terms of large-scale tectonics, it went along with Oligo-Miocene back-arc extension. However, this extension in the Cyclades was not principally controlled by simple shear in the middle and lower crust (e.g. Vandenberg and Lister 1996; Huet et al. 2009), but was associated with a large amount of near-coaxial stretching. This is more in line with a kinematic scenario that minimizes offsets along several generations of second-order detachment faults (HSZ, AF, CFS; see Fig. 2) with different senses of shear and times of operation (see, e.g., Vandenberg and Lister 1996; Thomson et al. 2009). The whole process of extension, on the other hand, led to a bulk vertical attenuation of the upper and middle Aegean crust of about 46 %.

Implications for the large-scale dynamics of the Aegean

On the basis of refraction seismic and gravimetric data, the Moho in the Cycladic region is estimated to be presently at about 26–30 km depth (lowermost cross section in Fig. 11; see also van der Maar 1980 and references therein). Removing the effect of coaxial extension and vertical attenuation above the BU on Ios Island, this would result in a 50-km-thick crust in the Eocene, with high palaeotopography, for which evidence is lacking. On the other hand, such a Moho depth has been assumed as a boundary constraint for numerical modelling (e.g. Huet et al. 2010). Thickened crust, however, had probably developed by subduction-related underthrusting of the CBS beneath the Pelagonian Unit (PU) in the Mesohellenic subduction-accretion setting (upper cross section in Fig. 11). Upward return flow of high-pressure units (eclogites, blueschists) in the CBS subduction channel may explain the close structural association with structural units (mainly metasediments) that lack evidence for a high-pressure overprint on many of the Cyclades islands (e.g. Trotet et al. 2001; Ring et al. 2010). The following collision and north-directed underthrusting of the Cycladic Basement Unit beneath CBS and PU units explains the greenschist-grade medium-pressure metamorphism on Ios and the partly higher-grade overprint on Naxos further north (second cross section from top; Fig. 11). In the Miocene, bivergent N–S extension led to basement extraction and to the formation of

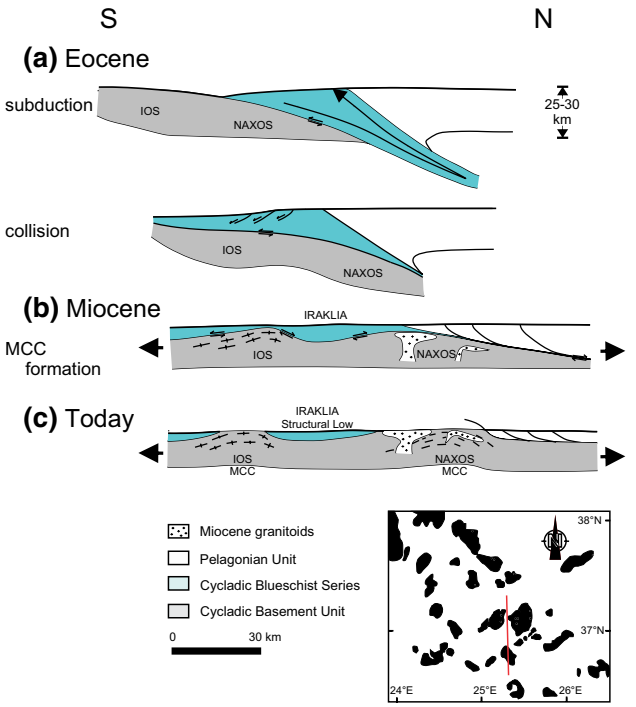

Fig. 11 Kinematic model for the southern and central Cyclades in the Aegean Sea, eocene to present. **a** Eocene; high-pressure metamorphism of CBS units in a north-dipping subduction channel (*blue*), followed by upward flow of material to mid-crustal levels. At collision, the extending CBS (*blue*) is emplaced on top of the BU. **b** Miocene; formation of the Ios MCCs accompanied by bivergent N–S extension. The SCSZ and second-order detachment faults aid in unroofing the BU. A top-to-north detachment juxtaposes the middle/lower crust and the upper crust of Naxos. **c** Today; extended and exhumed MCC of Ios and Naxos, with intermittent structural low defined by the CBS units (*blue*) on the Small Cyclades island of Iraklia

the metamorphic core complexes (e.g. Forster and Lister 1999a; Thomson et al. 2009) in the Cyclades (third cross section from top; Fig. 11). In places the previous thrust contact was reactivated as extensional detachments. This process was associated with significant thinning of the tectonic hangingwall units (the CBS and, further north, the PU) and ductile stretching of the BU on Ios (this study) and Naxos (e.g. Cao et al. 2013). Partial melting and the formation of granitoids are restricted to Naxos and partly outlasted extensional deformation in the basement there (e.g. Keay et al. 2001). The general geometry of the Miocene detachment system (Fig. 11) also constrains a major structural low between the islands of Ios and Naxos in the area of the Small Cyclades, where parts of the CBS with a specific high-pressure deformational overprint are preserved (Behrmann and Seckel 2007). Finally, it can also be stated that the contact between the BU and the CBS has seen an intensive extensional overprint in the Miocene, but must have initially been the site of overthrusting, as proposed by Huet et al. (2009).

Conclusion

The results of strain analysis and data on flow kinematics of the Cycladic Basement Unit exposed on Ios lead to the following conclusions:

1. The basement on Ios was stretched by about 70 % in N–S direction and flattened by about 40 % normal to the foliation in a plane strain environment ($k = 0.99$). A gradual decrease in strain down-section away from the South Cyclades Shear Zone (SCSZ) attests to the kinematic nature of this structure as a zone of ductile extension.
2. The rotational component of flow does not strongly deviate from pure shear (kinematic vorticity number $W_k = 0.26$ on average). The non-coaxial part of shearing suggests that there has been relative movement on the order of ten kilometres between the deeper parts of the basement and the hangingwall made up by the Cycladic Blueschist Series.
3. Because strain magnitude and W_k do not correlate, the Ios basement and the overlying units were stretched compatibly, allowing in principle to assess the amount of Miocene thinning of the upper and middle crust in the Cyclades.
4. Strain and flow kinematics on Ios do not support a tectonic model considering the SCSZ as a thrust structure. However, there must be an earlier history of this tectonic contact as an overthrust, owing to the occurrence of high-pressure rocks in the hangingwall unit.
5. The SCSZ formed part of a much larger system of Miocene-age detachments in the Aegean. Almost pureshear flow in the basement and bivergent (top-to-north and top-to-south) operation of shear zones on Ios indicates that extension in this area is dominantly coaxial, significantly reducing the tectonic overburden, but limiting the formation of discrete detachments.

Acknowledgments This work profited from intensive discussions with Gordon Lister and Erik Duesterhoeft that helped to sharpen our thinking. Constructive and detailed reviews by David Iacopini and Uwe Ring, as well as editorial advice by Paris Xypolias, helped to improve an earlier version of the manuscript. Kiriakos Batsalis is especially acknowledged for invaluable logistical support during our stays on Ios Island in the years 2013 and 2014.

References

Altherr R, Kreuzer H, Wendt J, Lenz H, Wagner GA, Keller J, Harre W, Hühndorf A (1982) A late Oligocene/early Miocene high temperature belt in the Attic-Cycladic crystalline complex (SE Pelagonian Greece). Geol Jahrb E23:97–164

Andriessen PAM, Banga G, Hebeda EH (1987) Isotopic age study of pre-Alpine rocks in the basal units on Naxos, Sikinos and Ios, Greek Cyclades. Geol Mijnb 66:3–14

Baldwin SL, Lister GS (1998) Thermochronology of the South Cyclades Shear Zone, Ios, Greece; effects of ductile shear in the argon partial retention zone. J Geophys Res 103:7315–7336. doi:10.1029/97JB03106

Behrmann JH (1987) A precautionary note on shear bands as kinematic indicators. J Struct Geol 9:659–666

Behrmann JH (1990) Gefügeuntersuchungen im KTB-Lokationsgebiet Oberpfalz (Geothermiebohrungen, Vorbohrung, Hauptbohrung, Aufschlüsse). DFG-Abschlussbericht. Albert-Ludwigs-Universität Freiburg, Giessen

Behrmann JH, Seckel C (2007) Structures, flow stresses, and estimated strain rates in metamorphic rocks of the Small Cyclades Islands Iraklia and Schinoussa (Aegean Sea, Greece). Geotecton Res 95:1–11

Boyer SE, Elliott D (1982) Thrust systems. AAPG Bull 66:1196–1230

Cao S, Neubauer F, Bernroider M, Liu J (2013) The lateral boundary of a metamorphic core complex: the Moutsounas shear zone on Naxos, Cyclades, Greece. J Struct Geol 54:103–128. doi:10.1016/j.jsg.2013.07.002

Coney PJ (1980) Cordilleran metamorphic core complexes: an overview. Geol Soc Am Mem 153:7–31

Dürr S, Altherr R, Keller J, Okrusch M, Seidel E (1978) The median Aegean crystalline belt: stratigraphy, structure, metamorphism, magmatism. In: Roeder HC, Schmidt K (eds) Alps. Appenines, Hellenides, Stuttgart, pp 455–477

Feehan JG, Brandon MT (1999) Contribution of ductile flow to exhumation of low-temperature, high-pressure metamorphic rocks: San Juan-Cascade nappes, NW Washington-State. J Geophys Res 104:10883–10902

Flinn D (1962) On folding during 3-D progressive deformation. Q J Geol Soc Lond 118:345–428

Forster MA, Lister GS (1996) Evolution of the Ios upper plate. Traverse 5–Varvara boudin to the 'Goat Beach'. In: Lister GS, Forster MA (eds) Inside the Aegean metamorphic core complexes, vol 45. Technical Publication Australian Crustal Research Centre, Monash University, Melbourne, pp 53–59

Forster MA, Lister GS (1999a) Detachment faults in the Aegean core complex of Ios, Cyclades, Greece. In: Ring U, Brandon MT, Lister GS, Willett SD (eds) Exhumation processes: normal faulting, ductile flow and erosion: geological society special publications. Geological Society, London, pp 305–323

Forster MA, Lister GS (1999b) Separate episodes of eclogite and blueschist facies metamorphism in the Aegean metamorphic core complex of Ios, Cyclades, Greece. In: Ring U, Brandon MT, Lister GS, Willett SD (eds) Exhumation processes: normal faulting, ductile flow and erosion: geological society special publications, vol 164. Geological Society, London, pp 157–177

Fry N (1979a) Random point distributions and strain measurement in rocks. Tectonophysics 60:89–105

Fry N (1979b) Density distribution techniques and strained length methods for determination of finite strains. J Struct Geol 1:221–229

Gerya TV, Stoeckhert B, Perchuk AL (2002) Exhumation of high-pressure metamorphic rocks in a subduction channel: a numerical simulation. Tectonics 21:1–19. doi:10.1029/2002TC001406

Ghosh SK, Ramberg H (1976) Reorientation of inclusions by combination of pure shear and simple shear. Tectonophysics 34:1–70

Grasemann B, Schneider DA, Stöckli DF, Iglseder C (2012) Miocene bivergent crustal extension in the Aegean: evidence from the western Cyclades (Greece). Lithosphere 4:23–39

Henjes-Kunst F (1980) Alpidische Einformung des präalpidischen Kristallins und seiner mesozoischen Hülle auf Ios (Kykladen,

Griechenland). Unpublished Ph.D. Thesis, University of Braunschweig, Germany
Henjes-Kunst F, Kreuzer H (1982) Isotopic dating of pre-alpidic rocks from the Island of Ios (Cyclades, Greece). Contrib Mineral Petrol 80:245–253. doi:10.1007/BF00371354
Holcombe R (2004) GeoFryPlots 3.1. http://www.holcombe.net.au/software/downloads/GeoFryPlots_zip.exe. Accessed 18 July 2014
Huet B, Labrousse L, Jolivet L (2009) Thrust or detachment? Exhumation processes in the Aegean: insight from a field study in Ios (Cyclades, Greece). Tectonics 28:3. doi:10.1029/2008TC002397
Huet B, Pourhiet LL, Labrousse L, Burov E, Jolivet L (2010) Post-orogenic extension and metamorphic core complexes in a heterogeneous crust: the role of crustal layering inherited from collision. Application to the Cyclades (Aegean domain). Geophys J Int 184:611–625
Iacopini D, Carosi R, Montomoli C, Passchier CW (2008) Strain analysis of flow in the Northern Sardinian Variscan Belt: recognition of a partitioned oblique deformation event. Tectonophysics 446:77–96
Jacobshagen V (1986) Geologie von Griechenland, vol 19. Gebrueder Borntraeger Verlagsbuchhandlung, Berlin
Jansen JBH, Schuiling RD (1976) Metamorphism on Naxos: petrology and geothermal gradients. Am J Sci 276:1225–1253
Jeffery GB (1922) The motion of ellipsoidal particles immersed in a viscous fluid. In: Proceedings of the Royal Society, London A102, pp 161–179
Johnson SE, Lenferink HJ, Price NA, Marsh JH, Koons PO, West DP Jr, Beane R (2009) Clast-based kinematic vorticity gauges: the effects of slip at matrix/clast interfaces. J Struct Geol 31:1322–1339
Jolivet L, Faccenna C, Huet H, Labrousse L, Le Pourhiet L, Lacombe O, Lecomte E, Burov E, Denèle Y, Brun JP, Philippon M, Paul A, Salaün G, Karabulut H, Piromallo C, Monié P, Gueydan F, Okay A, Oberhänsli R, Pourteau A, Augier R, Gadenne L, Driussi O (2012) Aegean tectonics: strain localisation, slab tearing and trench retreat. Tectonophysics. doi:10.1016/j.tecto.2012.06.011
Keay S, Lister GS, Buick I (2001) The timing of partial melting, Barrovian metamorphism and granite intrusion in the Naxos metamorphic core complex, Cyclades, Aegean Sea, Greece. Tectonophysics 342:275–312
Kilias A, Falalakis G, Mountrakis D (1999) Cretaceous-Tertiary structures and kinematics of the Serbomacedonian metamorphic rocks and their relation to the exhumation of the Hellenic hinterland (Macedonia, Greece). Int J Earth Sci 88:513–531
Kumerics C, Ring U, Brichau S, Glodny J, Monié P (2005) The extensional Messaria shear zone and associated brittle detachment faults, Aegean Sea, Greece. J Geol Soc 162:701–721
Le Pichon X, Angelier J (1979) The Hellenic arc and trench system: a key to the neotectonic evolution of the eastern Mediterranean area. Tectonophysics 60:1–42
Lister GS, Davis GA (1989) The origin of metamorphic core complexes and detachment faults formed during Tertiary continental extension in the northern Colorado River region, USA. J Struct Geol 11:65–94
Lister GS, Keay S (1996) The lower plate of the Ios core complex. Traverse 2–Mylopotas Beach to the South Headland. In: Lister GS, Forster MA (eds) Inside the Aegean metamorphic core complexes, vol 45. Technical Publication Australian Crustal Research Centre, Monash University, Melbourne, pp 35–39
Lister GS, Snoke AW (1984) SC mylonites. J Struct Geol 6:617–638
Lister GS, Banga G, Feenstra A (1984) Metamorphic core complexes of cordilleran type in the Cyclades, Aegean Sea, Greece. Geology 12:221–225. doi:10.1130/0091-7613(1984)12<221:MCCOCT>2.0.CO;2
Passchier CW (1987) Stable positions of rigid objects in non-coaxial flow–a study in vorticity analysis. J Struct Geol 9:679–690
Piazolo S, Bons PD, Passchier CW (2002) The influence of matrix rheology and vorticity on fabric development of populations of rigid objects during plane strain deformation. Tectonophysics 351:315–329
Platt JP, Vissers RLM (1980) Extensional structures in anisotropic rocks. J Struct Geol 2:397-410
Ramsay JG, Graham RH (1970) Strain variations in shear belts. Can J Earth Sci 7(3):786–813. doi:10.1139/e70-078
Ramsay JG, Huber MI (1983) The techniques of modern structural geology. Strain analysis, vol 1. Academic Press, London
Ring U, Kumerics C (2008) Vertical ductile thinning and its contribution to the exhumation of high-pressure rocks: the Cycladic blueschist unit in the Aegean. J Geol Soc Lond 165:1019–1030
Ring U, Laws S, Bernet M (1999) Structural analysis of a complex nappe sequence and late-orogenic basins from the Aegean Samos Island, Greece. J Struct Geol 21:1575–1601
Ring U, Glodny J, Will T, Thomson SN (2010) The Hellenic subduction system: high-pressure metamorphism, exhumation, normal faulting, and large-scale extension. Annu Rev Earth Planet Sci 38:45–76
Schliestedt M, Altherr R, Matthews A (1987) Evolution of the Cycladic crystalline complex: petrology, isotope geochemistry and geochronology. In: Helgerson HC (ed) Chemical transport in metasomatic processes. D. Reidel, Dordrecht, pp 389–428
Seidel M, Zacher W, Schwarz WH, Jaeckel P, Reischmann T (2006) A Late Carboniferous age of the gneiss of Potamos (Kythira Island, Greece) and new considerations on geodynamic interpretations of the Western Hellenides. Neues Jahrb Geol Paläontol Abh 241:325–344
Shreve RL, Cloos M (1986) Dynamics of sediment subduction, melange formation, and prism accretion. J Geophys Res 91:10229–10245. doi:10.1029/JB091iB10p10229
Thomson SN, Ring U, Brichau S, Glodny J, Will TM (2009) Timing and nature of formation of the Ios metamorphic core complex, southern Cyclades, Greece. Geol Soc Lond (Special Publications) 321(1):139–167
Trotet F, Jolivet L, Vidal O (2001) Tectono-metamorphic evolution of Syros and Sifnos islands (Cyclades, Greece). Tectonophysics 338(2):179–206
van der Maar PA (1980) The geology and petrology of Ios. Cyclades Greece Ann Geol Pays Helleniques 30:206–224
van der Maar PA, Jansen BH (1983) The geology of the polymetamorphic complex of Ios. Cyclades, Greece and its significance for the Cycladic Massif. Geol Rundsch 72:283–299. doi:10.1007/BF01765910
van der Maar PA, Vink BW, Jansen BH (1981) Ios, geological map, scale 1:50,000. Institute of Geology and Mining Explorer, Athens, Greece
Vandenberg LC, Lister GS (1996) Structural analysis of basement tectonics from the Aegean metamorphic core complex of Ios. Cyclades. Greece J Struct Geol 18:1437–1454. doi:10.1016/S0191-8141(96)00068-5
Xypolias P (2010) Vorticity analysis in shear zones: a review of methods and applications. J Struct Geol 32:2072–2092. doi:10.1016/j.jsg.2010.08.009